ACS OMEGA

Open Access

http://pubs.acs.org/journal/acsodf

Article

Decorating $Mg_{12}O_{12}$ Nanocage with Late First-Row Transition Metals To Act as Single-Atom Catalysts for the Hydrogen Evolution Reaction

Abdulrahman Allangawi, Naveen Kosar, Khurshid Ayub, Mazhar Amjad Gilani, Nur Hazimah Binti Zainal Arfan, Malai Haniti Sheikh Abdul Hamid, Muhammad Imran, Nadeem S. Sheikh,* and Tariq Mahmood*

Cite This: *ACS Omega* 2023, 8, 37820−37829

Read Online

ACCESS | Metrics & More | Article Recommendations | Supporting Information

ABSTRACT: In the pursuit of sustainable clean energy sources, the hydrogen evolution reaction (HER) has attained significant interest from the scientific community. Single-atom catalysts (SACs) are among the most promising candidates for future electrocatalysis because they possess high thermal stability, effective electrical conductivity, and excellent percentage atom utilization. In the present study, the applicability of late first-row transition metals (Fe-Zn) decorated on the magnesium oxide nanocage (TM@$Mg_{12}O_{12}$) as SACs for the HER has been studied, via density functional theory. The late first-row transition metals have been chosen as they have high abundance and are relatively low-cost. Among the studied systems, results show that the Fe@$Mg_{12}O_{12}$ SAC is the best candidate for catalyzing the HER reaction as it exhibits the lowest activation barrier for HER. Moreover, Fe@$Mg_{12}O_{12}$ shows high stability (E_{int} = −1.64 eV), which is essential in designing SACs to prevent aggregation of the metal. Furthermore, the results of the electronic properties' analysis showed that the HOMO−LUMO gap of the nanocage is decreased significantly upon doping of Fe (from 4.81 to 2.28 eV), indicating an increase in the conductivity of the system. This study highlights the potential application of the TM@nanocage SAC systems as effective HER catalysts.

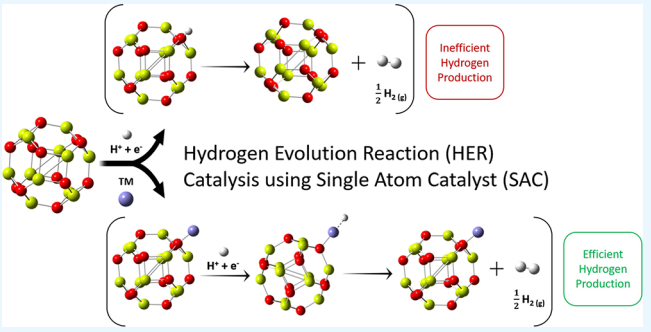

1. INTRODUCTION

One of the most promising alternative to fossil fuels is the hydrogen fuel.[1−3] Fossil fuels cause devastating effects on climate change, whereas hydrogen can be used to obtain clean energy with only water as the byproduct.[4] Moreover, hydrogen has a high gravimetric energy density (142 MJ kg^{-1}), which is three times higher than that of gasoline.[5] Hydrogen can be stored either in a liquid form (cryogenic) or as metal hydrides and can be transported over long distances.[6−8] Hydrogen can be produced by several processes such as the reforming of light hydrocarbons in biomass,[9] natural gas,[10] coal,[11] petroleum,[12] and water electrolysis.[13] Hydrogen evolution from electrochemical water splitting using renewable resource-derived electricity is a very promising technology among the mentioned techniques.[14−17]

Water electrolysis includes two half-cell reactions: the hydrogen evolution reaction (HER) and the oxygen evolution reaction (OER).[18] The advantages of utilizing the HER include the high purity of the produced hydrogen as well as the use of water as the reactant.[19−23] The main disadvantage of the HER is the activation barrier of the reaction and therefore its high overpotential.[24] To overcome this problem, highly efficient catalysts are required to lower the activation barrier of the reaction.[25]

Single-atom catalysts (SACs) are among the most promising candidates for electrocatalysis because they possess high thermal stability, effective electrical conductivity, and provide excellent percentage atom utilization.[26] SACs are synthesized by dispersing metal atoms on appropriate supports to create single-atom catalytic sites. This leads to almost 100% metal utilization due to exposure of most number of metal atoms as active sites.[27,28] Precious metals, and more specifically Pt-based electrocatalysts, have proven to be best for catalyzing the HER. Unfortunately, the high cost of Pt limits its large-scale application.[29−31]

Application of non-precious metal SACs for the HER has recently gained the focus of the scientific community.[32,33]

Received: March 16, 2023
Accepted: June 9, 2023
Published: October 8, 2023

Among these non-precious metals, a lot of research has been conducted to search for low-cost abundant transition metals (TMs), more specifically late first-row TM-based SACs.[34−39] For instance, Sun et al.[40] investigated the HER catalysis performance of late first-row TMs on the SnO 2D monolayer. They found out experimentally that Co, Ni, and Cu had the best SAC performance with Gibbs free energies of hydrogen evolution (ΔG_{H^*}) almost equal to zero, especially with Co (ΔG_{H^*} = 0.015 eV). This result is competitive with the benchmark results for Pt (ΔG_{H^*} = −0.09 eV). Moreover, Qiu et al.[36] anchored nickel atoms onto a three-dimensional nonporous graphene material and examined the catalytic activity for the HER. The researchers showed that the material catalyzes the HER with low overpotentials. Theoretical investigations revealed that sp−d charge transfer between nickel and the surrounding carbon atom results in hybrid orbitals that are catalytically active. Furthermore, Fei et al.[38] dispersed cobalt atoms on nitrogen-doped graphene and evaluated its catalytic capability toward the HER. The results showed that the proposed catalyst is highly active with very low overpotentials. The researchers concluded that the interaction of the metal atom with the nitrogen atoms within the support enhanced the catalytic activity of the active site.

Support materials play a more vital role than merely increasing the atom utilization efficiency. They can enhance the HER catalysis capability of the metal centers.[20,41,42] Therefore, much care must be taken while considering a support. Some properties of the support such as the presence of defects and edges, high electrical conductivity, high chemical stability, and large surface area can enhance the catalytic activity of the designed catalyst. Edges and corners in the support provide binding sites for metal adsorption, the high electrical conductivity in the support facilitates electron transfer, the high chemical stability ensures that the support remains intact during the harsh conditions of electrocatalysis, and the high surface area helps dispersing metal atoms evenly and avoid aggregation.[26,43,44]

Recently, wide applicability of $Mg_{12}O_{12}$ has been witnessed in chemical sensing, drug delivery, non-linear optics, and hydrogen storage.[45−50] For instance, Ghorbanzadeh Ahangari and Hamed Mashhadzadeh[50] investigated several C_{24} nanocage analogues, namely, C_{24}, $B_{12}N_{12}$, Al_{12} N_{12}, $Be_{12}O_{12}$, $Mg_{12}O_{12}$, and $Zn_{12}O_{12}$ for hydrogen storage; the researchers concluded that $Mg_{12}O_{12}$ and $Zn_{12}O_{12}$ are best at storing hydrogen (up to four hydrogen molecules per nanocage). Moreover, Fallahi et al.[47] examined the efficiency of $Be_{12}O_{12}$, $Mg_{12}O_{12}$, and $Zn_{12}O_{12}$ nanocages toward the drug delivery of the anticancer drug hydroxyurea. Results showed that $Mg_{12}O_{12}$ is the best candidate for the adsorption and desorption of tabun drugs. Furthermore, Shakerzdeh et al.[49] studied Li, Na, and K decorated on $Mg_{12}O_{12}$ and $Be_{12}O_{12}$ nanocages as non-linear optics. The encapsulation of the Li atom inside $Mg_{12}O_{12}$ was shown to enhance the hyperpolarizability of the nanocage and remarkably narrow down the HOMO−LUMO gap. Hussain et al.[51] theoretically proposed Zn-decorated $Mg_{12}O_{12}$ nanoclusters and suggested the use of these clusters as high-performance $COCl_2$ sensing materials.

The $Mg_{12}O_{12}$ nanocage contains desirable properties to act as a support in SACs. It has high stability, contains lots of edges, and decorating late first-row TMs on it was shown to increase its E_{gap}.[45,46] However, to the best of our knowledge, no studies have been published on utilizing TM-doped $Mg_{12}O_{12}$ nanocages (TM@$Mg_{12}O_{12}$) as SACs. Herein, we utilize density functional theory (DFT) calculations to study the stability, the electronic properties, and the HER catalytic performance of late first-row TMs (Fe-Zn) supported on the $Mg_{12}O_{12}$ nanocage. The choice of examining late first-row TMs as opposed to precious/noble earth metals was made in order to design a more sustainable, affordable, and potentially scalable HER catalyst, where late first-row TMs are significantly more affordable as compared to precious/noble metals. Moreover, numerous studies have shown the potential applicability of late first-row TM SACs for the HER.[26]

2. RESULTS AND DISCUSSION

The geometry of the pristine $Mg_{12}O_{12}$ nanocage has been optimized by using DFT calculations (Figure 1). The nanocage

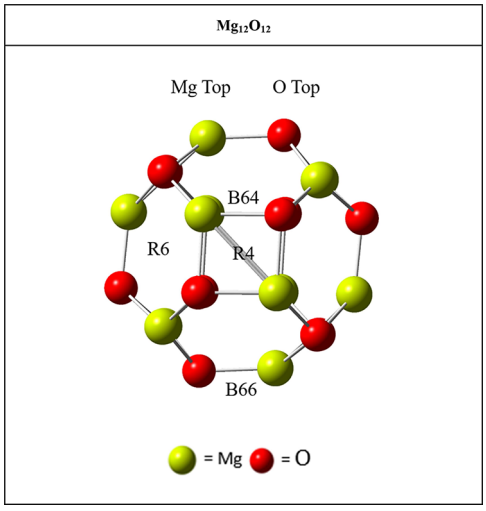

Figure 1. Optimized structure of the magnesium oxide ($Mg_{12}O_{12}$) nanocage. The O top, Mg top, R6, R4, B66, and B64 sites are above the oxygen atom, above the magnesium atom, in the middle of the 6-membered ring, in the middle of the 4-membered ring, above the bond within the 6-membered rings, and above the bond shared by the 6- and 4-membered rings, respectively.

structure consists of eight 6-membered rings and six 4-membered rings. In the optimized geometry, the Mg−O bond length in the 6-membered and 4-membered rings is 1.89 and 1.95 Å, respectively. These values are consistent with previously reported data, validating the reliability of the method.[49,50] Analysis of the $Mg_{12}O_{12}$ nanocage reveals six distinct binding sites for the decoration of TMs (Figure 1). To find the most suitable site for doping of TMs, all six configurations of the TM@$Mg_{12}O_{12}$ complex have been modeled and optimized. After optimization, all six configurations converged to the oxygen top position, and the corresponding structures are shown in Figure 2 for each metal. The preferability of the TMs to the oxygen top position is somewhat expected because first-row TMs are electropositive in nature,[52] and by a common reason, they are attracted to the strongly electronegative oxygen atom. Moreover, Shakerzdeh et al.[49] reported the same behavior with the doping of Li, Na, and K atoms on the $Mg_{12}O_{12}$ nanocages. Furthermore, the convergence of the TMs from all sites toward the oxygen top site indicates that the diffusion of the TMs to other sites is highly unfavorable.

TM atoms can adopt several spin states as they contain valance electrons in d-orbitals. Valance electrons in d-orbitals

https://doi.org/10.1021/acsomega.3c01794
ACS Omega 2023, 8, 37820−37829

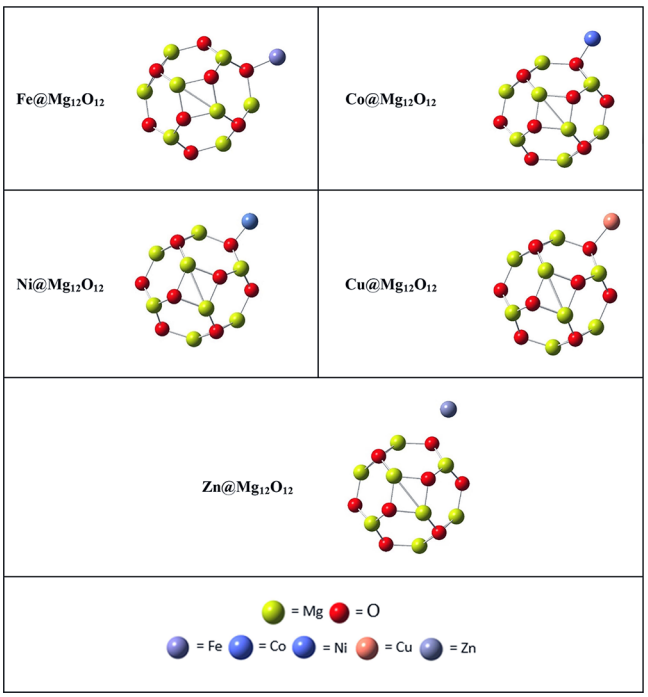

Figure 2. Optimized structures of $TM@Mg_{12}O_{12}$.

can exist as pairs when the corresponding energies of the orbitals are far apart or they can reside as unpaired electrons when the orbitals have similar energies.[52] To ensure that the best spin state is chosen, spin-polarized calculations are performed, and only the most stable spin state is considered for further analysis. Table 1 shows the spin states for each TM. It is observed that differences in energies between the spin states are as large as 8.94 eV, which highlights the importance of conducting spin-polarized calculations. The most stable states for $Fe@Mg_{12}O_{12}$, $Co@Mg_{12}O_{12}$, $Ni@Mg_{12}O_{12}$, $Cu@Mg_{12}O_{12}$, and $Zn@Mg_{12}O_{12}$ are the quintet, quartet, singlet, doublet, and singlet spin state, respectively.

Stabilities of SACs supported on the $Mg_{12}O_{12}$ nanocage have been estimated by calculating the interaction energy of each complex. Negative values of interaction energies indicate the stability of the structures; in other words, a more negative value of interaction energy implies greater stability. Interaction energies are listed in Table 2; it is seen that all $TM@Mg_{12}O_{12}$ SACs have negative interaction energies, indicating the stability of these complexes. $Co@Mg_{12}O_{12}$ is the most stable structure (−2.52 eV), followed by $Fe@Mg_{12}O_{12}$ and $Ni@Mg_{12}O_{12}$ (−1.64 and −1.49 eV, respectively) and then $Cu@Mg_{12}O_{12}$ (−1.09 eV) and $Zn@Mg_{12}O_{12}$ (−0.42). To ensure that metal atoms in the SACs get dispersed properly on the support and avoid aggregation, interaction energies should be lower than the TM−TM bond. Therefore, SACs with lower interaction

Table 2. Interaction Energies (in eV), Energies of HOMOs, LUMOs, HOMO−LUMO Energy Gap (in eV), and NBO Charge on Metals in the SAC (in |e|)

system	E_{int}	E_{HOMO}	E_{LUMO}	E_{gap}	Q_{TM}
$Mg_{12}O_{12}$		−6.59	−1.78	4.81	
$Fe@Mg_{12}O_{12}$	−1.64	−4.18	−1.90	2.28	0.045
$Co@Mg_{12}O_{12}$	−2.52	−4.13	−1.86	2.27	0.032
$Ni@Mg_{12}O_{12}$	−1.49	−4.78	−1.88	2.90	0.033
$Cu@Mg_{12}O_{12}$	−1.09	−3.93	−1.85	2.09	0.021
$Zn@Mg_{12}O_{12}$	−0.42	−4.89	−1.91	2.99	0.041

energies are expected to be more efficient and have finely dispersed single-atom sites.[26] Strong interaction energies of $Co@Mg_{12}O_{12}$, $Fe@Mg_{12}O_{12}$, and $Ni@Mg_{12}O_{12}$ suggest that dispersing these metals on the $Mg_{12}O_{12}$ support will be facilitated. However, caution must be taken with $Cu@Mg_{12}O_{12}$ and more so with $Zn@Mg_{12}O_{12}$ when synthesizing them due to the possibility of aggregation. The values of adsorption energies in this study are in line with various studies in the literature.[40,53−55]

Analysis of frontier molecular orbitals (FMOs) was performed to investigate the impact of adsorbing the TMs on the electronic environment of the nanocage. Energies of the highest occupied molecular orbital (HOMO), lowest unoccupied molecular orbital (LUMO), and the E_{gap} are shown in Table 2. In electrocatalysts, low E_{gap} values are desirable as they enhance the conductivity of the catalyst.[56] The E_{gap} for $Mg_{12}O_{12}$ is 4.81 eV, which indicates its semi-conducting behavior. Moreover, the obtained E_{gap} value is consistent with the previously reported values in the literature,[48−50,57−59] validating the electronic analysis results. Upon adsorption, the smallest E_{gap} is shown for $Cu@Mg_{12}O_{12}$ (E_{gap} = 2.09 eV) followed by $Co@Mg_{12}O_{12}$ (E_{gap} = 2.27 eV), $Cu@Mg_{12}O_{12}$ (E_{gap} = 2.28 eV), $Ni@Mg_{12}O_{12}$ (E_{gap} = 2.90 eV), and finally $Zn@Mg_{12}O_{12}$ (E_{gap} = 2.99 eV). The decrease in E_{gap} is attributed to the increase of the HOMO energy of the doped systems, while the LUMOs had little to no change in energy (except for $Zn@Mg_{12}O_{12}$). Overall, the large decrease of E_{gap} observed for all designed catalysts reflects the enhancement of conductivity upon doping of the TMs. Graphical analysis of the HOMO and LUMO isosurfaces is shown in Figure 3 (refer to the Supporting Information, Figure S1 for all metals). It is shown that the HOMO of $TM@Mg_{12}O_{12}$ systems is located mostly on the respective TMs, while in the pristine $Mg_{12}O_{12}$, it is distributed throughout the nanocage. The density of states (DOS) spectra are shown in Figure 4 (refer to the Supporting Information, Figure S2 for the other metals). Comparison of the pristine and TM-doped $Mg_{12}O_{12}$ spectra shows new orbitals in the region between −6.00 and −3.00 eV in $TM@Mg_{12}O_{12}$; these new orbitals have contributions almost entirely from the TM. We can conclude that the increase of energy in the HOMO of $TM@Mg_{12}O_{12}$ is attributed to new orbitals

Table 1. Relative Energies (E_{rel}) of Different Spin States of Fe-Zn Adsorbed on $Mg_{12}O_{12}$ (Energies in eV)

stable spin state	$Fe@Mg_{12}O_{12}$	$Co@Mg_{12}O_{12}$	$Ni@Mg_{12}O_{12}$	$Cu@Mg_{12}O_{12}$	$Zn@Mg_{12}O_{12}$
most stable	quintet	quartet	singlet	doublet	singlet
2nd stable	triplet	doublet	triplet	quartet	triplet
3rd stable	singlet	sextet	quintet	sextet	quintet
E_{rel} of most stable	0.00	0.00	0.00	0.00	0.00
E_{rel} of 2nd stable	0.85	0.01	0.10	4.02	2.43
E_{rel} of 3rd stable	2.63	2.21	3.04	8.94	6.73

https://doi.org/10.1021/acsomega.3c01794
ACS Omega 2023, 8, 37820−37829

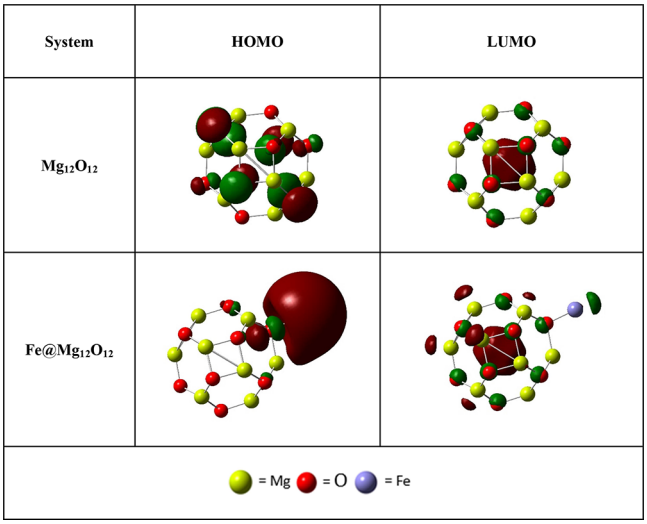

Figure 3. Graphical representation of the HOMOs and LUMOs of $Mg_{12}O_{12}$ and $Fe@Mg_{12}O_{12}$.

introduced by the TM atoms. The densities of the LUMOs are similar in pristine and $TM@Mg_{12}O_{12}$ spectra; they are located mostly on the nanocages with slight densities present on the TMs.

The natural bond orbital (NBO) analysis has been done on the designed SACs to quantify the charge transfer between the $Mg_{12}O_{12}$ support and TMs.[60,61] NBO charges on TMs can be seen in Table 2. It is expected that metal atoms will have large positive values due to their electropositive nature.[52] However, the charges on the TMs in the $TM@Mg_{12}O_{12}$ complexes are in the range of 0.021−0.045 |e|. These values indicate that only a slight amount of charge has been transferred from the TM to the support. This might be attributed to the fact that oxygen atoms in the pristine $Mg_{12}O_{12}$ have large negative NBO charges, to begin with (−1.634 |e|). A literature search revealed that similar results have been found with decorating first-row TMs on a boron phosphide nanocage ($B_{12}P_{12}$).[62]

To optimize the structures of the hydrogen adsorbed intermediates (H^*-$TM@Mg_{12}O_{12}$), hydrogen is placed in the TM region, and it is allowed to converge. The optimized geometries of the intermediates are shown in Figure 5. To

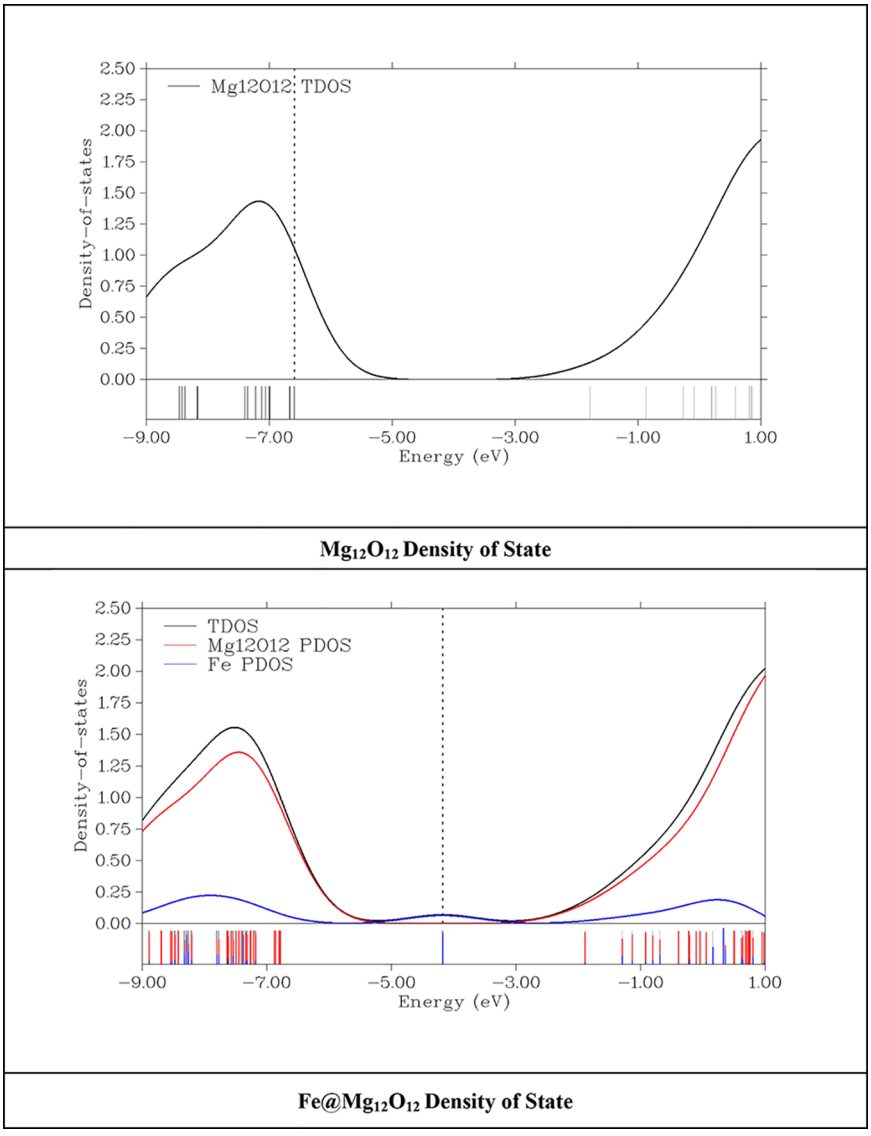

Figure 4. TDOS and PDOS of $Mg_{12}O_{12}$ and $Fe@Mg_{12}O_{12}$.

https://doi.org/10.1021/acsomega.3c01794
ACS Omega 2023, 8, 37820−37829

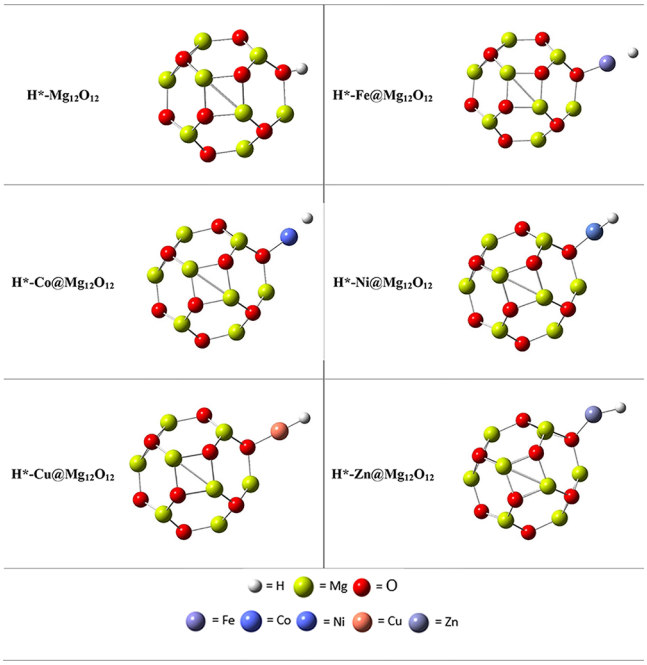

Figure 5. Optimized geometries of the HER intermediates.

evaluate the stabilities of H*-TM@$Mg_{12}O_{12}$ intermediates, interaction energies are calculated and shown in Table 3. The

Table 3. Adsorption Energies and Gibbs Free Energies of Hydrogen Evolution Adsorption (eV)

system	E_{H^*}	ΔG_{H^*}
H*-$Mg_{12}O_{12}$	1.19	1.42
H*-Fe@$Mg_{12}O_{12}$	−0.77	−0.56
H*-Co@$Mg_{12}O_{12}$	−1.06	−0.89
H*-Ni@$Mg_{12}O_{12}$	−1.05	−0.83
H*-Cu@$Mg_{12}O_{12}$	−1.28	−1.08
H*-Zn@$Mg_{12}O_{12}$	0.64	0.80

interaction energies of the H*-TM@$Mg_{12}O_{12}$ intermediates corresponding to the Fe-Cu metals have negative values, indicating the stability of each complex. However, the interaction energy of the H*-Zn@$Mg_{12}O_{12}$ complex is positive (0.64 eV), indicating that the complex formed will be unstable. Moreover, to ensure that hydrogen preferably adsorbs on the active TM sites rather than being strongly attached to the nanocage surface, the interaction energy of hydrogen with the pristine nanocage (H*-$Mg_{12}O_{12}$) is calculated. All six binding sites (B66, B64, O top, Mg top, R6, and R4, see Figure 1) are investigated for hydrogen adsorption to the pristine nanocage. The most stable structure (Figure 6) has been determined to have hydrogen adsorbed on the O top position, which is similar to the adsorption of TMs on the nanocage (as discussed *vide supra*). The interaction energy of H*-$Mg_{12}O_{12}$ is largely positive (1.19 eV), indicating the instability of adsorbing hydrogen to the nanocage and thus preventing the hydrogen spillover effect.[63]

The activity of the designed SACs toward the HER is evaluated by calculating the Gibbs free energy of hydrogen evolution (ΔG_{H^*}). Negative values of ΔG_{H^*} correspond to favoring hydrogen adsorption, while positive values indicate difficulties in the adsorption. A good catalyst for the HER should have ΔG_{H^*} close to zero to enable both adsorption and

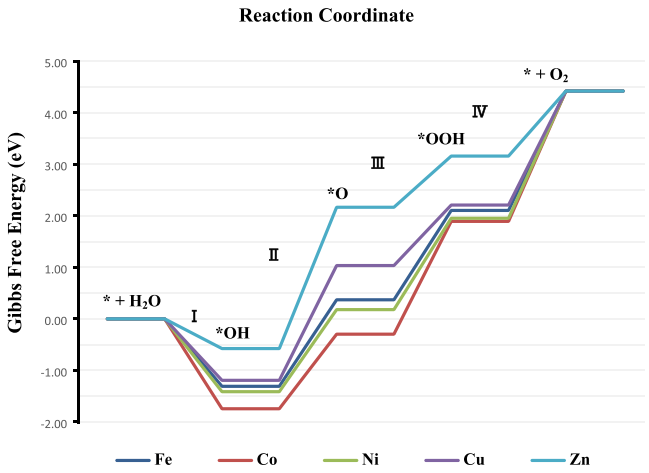

Figure 6. Gibbs free energy of all OER PCET steps.

desorption of hydrogen. Table 3 shows that the ΔG_{H^*} for H-*Fe@$Mg_{12}O_{12}$, H-*Co@$Mg_{12}O_{12}$, H-*Ni@$Mg_{12}O_{12}$, H-*Cu@$Mg_{12}O_{12}$, and H-*Zn@$Mg_{12}O_{12}$ SACs is −0.56, −0.89, −0.83, −1.08, and 0.80 eV, respectively. The SAC having the closest value to zero is Fe@$Mg_{12}O_{12}$, promoting it to be a feasible catalyst for the HER. Moreover, it is further confirmed that the adsorption of hydrogen on the undecorated nanocage site is thermodynamically unfavorable (ΔG_{H^*} = 1.42 eV). The HER activity of the proposed Fe@$Mg_{12}O_{12}$ catalyst is compared with other Fe-based SACs reported in the literature (Table 4).

Table 4. Comparison of Our Proposed Fe@$Mg_{12}O_{12}$ Catalyst with Other Fe-Based SACs[a]

SACs	ΔG_{H^*} (eV)	reference
Fe@$Mg_{12}O_{12}$	−0.56	our work
Fe@GY	−1.72	64
Fe@SnO	−0.44	40
Fe@Cr_2CO_2	−0.12	39
Fe@Mo_2CO_2	0.16	39
Fe@N_4	±0.20	65
Fe@GD	±0.07	66
Fe@NC	±0.11	67

[a]For experimental studies, the numerical value of ΔG_{H^*} is taken as ± the overpotential.

It can be seen in Table 4 that the Fe-based SACs have ΔG_{H^*} values ranging from magnitudes of 1.72 to 0.07 eV. The designed Fe@$Mg_{12}O_{12}$ catalyst in this study has slightly lower catalytic activity as compared to the best-reported catalysts. Results in this study have shown that the Fe@$Mg_{12}O_{12}$ system exhibits high stability, enhanced conductivity, resistance to the hydrogen spillover effect, and reasonable catalytic activity. Therefore, it is of wide interest to investigate other TM@$X_{12}Y_{12}$ systems as SACs.

The main goal of this study was to investigate the HER activity of the designed TM@$Mg_{12}O_{12}$ SACs. However, the applicability of the designed SACs toward the OER is briefly discussed in this part. The method outlined in our previous work[68] is applied here to examine the activity of the designed catalysts toward the OER. In short, the OER proceeds through four proton-coupled electron transfer (PCET) steps in neutral conditions (eqs I–IV).[69,70]

$$^*+H_2O \rightarrow {}^*OH + H^+ + e^- \quad \text{(I)}$$

https://doi.org/10.1021/acsomega.3c01794
ACS Omega 2023, 8, 37820−37829

$$^{*}OH \rightarrow {}^{*}O + H^{+} + e^{-} \quad (II)$$

$$^{*}O + H_2O \rightarrow {}^{*}OOH + H^{+} + e^{-} \quad (III)$$

$$^{*}OOH \rightarrow {}^{*} + O_2 + H^{+} + e^{-} \quad (IV)$$

where * and *X represent the active catalytic site and the OER intermediates, respectively. The overpotential of the OER depends on ΔG of the potential-determining step (PDS), which is defined as the PCET step with the largest ΔG. Therefore, by identifying the PDS, the associated ΔG (ΔG_{PDS}) and the overpotential (η_{OER}) can be calculated.

To find the most stable structures of the OER intermediates, spin-polarized calculations have been performed on all intermediates (Table S1). The optimized geometries of the OER intermediates are presented in Figure S3. Results of the thermodynamic calculation of ΔG for each PCET step are shown in Figure 6 (numerically in Table S2). Results show that for all designed catalysts, step I is exergonic, while all other PCET steps are endergonic. Although it would be ideal to have all PCET steps endergonic with the same numerical value, the thermodynamic stability of the OER intermediates differs by nature, making some steps exergonic while others are endergonic. Moreover, Table 5 highlights the PDS for each system, the associated ΔG_{PDS}, and η_{OER}. It is shown that for the Fe, Co, and Ni SACs, the PDS is step IV, while for Cu and Zn, it is step II. The best catalytic activity is shown by the Cu SAC, with ΔG_{PDS} and η_{OER} values of 2.23 eV and 1.11 V, respectively. However, these values are slightly higher than what is preferably obtained in the literature as feasible OER catalysts.[16]

Table 5. PDS of All Systems, the Associated Gibbs Free Energy Change, and the Overpotential

system	PDS	ΔG_{PDS} (eV)	η_{OER} (V)
$Fe@Mg_{12}O_{12}$	eq IV	2.32	1.21
$Co@Mg_{12}O_{12}$	eq IV	2.82	1.42
$Ni@Mg_{12}O_{12}$	eq IV	2.47	1.36
$Cu@Mg_{12}O_{12}$	eq II	2.23	1.11
$Zn@Mg_{12}O_{12}$	eq II	2.74	1.64

3. CONCLUSIONS

In conclusion, the magnesium oxide ($Mg_{12}O_{12}$) nanocage has been proposed as a suitable support for late first-row TM (Fe-Zn) single-atom catalysis of the HER. Stability, electronic, NBO, and thermodynamic analyses were performed to investigate the applicability of these SACs. Results revealed that $Fe@Mg_{12}O_{12}$ is the best candidate for catalyzing the HER, with the lowest Gibbs free energy of hydrogen evolution (ΔG_{H^*} = −0.56 eV). The Gibbs free energy of hydrogen evolution should be as close to zero as possible for a good catalyst. The major challenge in synthesizing SACs is the aggregation of the TM as clusters or nanoparticles instead of forming single-atom active sites. The interaction energy of $Fe@Mg_{12}O_{12}$ is the second highest (−1.64 eV) among the designed SACs; such a high value indicates the stability of the catalyst, which will facilitate the synthesis of the SAC. Moreover, the adsorption of Fe greatly increased the conductivity of the nanocage, facilitating its conductivity for electrocatalysis. This study illustrates the applicability of using the $Mg_{12}O_{12}$ nanocage as a support for designing SACs and encourages the investigation of other $TM@X_{12}Y_{12}$ systems as SACs.

4. COMPUTATIONAL METHODS EMPLOYED IN CURRENT WORK

All calculations have been executed by using Gaussian 09 software.[71] All structural modeling and visualization were performed using the GaussView 6.0.16 package.[72] The ωB97xD functional of DFT with the 6−31 + G(d,p) basis set was selected for geometry optimization, stability investigation, and thermodynamic evaluation. ωB97XD, a hybrid functional, was chosen to account for non-covalent interactions, including dispersion forces.[73] This functional has proven its reliability for studying HER SAC systems.[64] Frequency calculations have been performed on all structures to verify that they are true minima and not saddle points (no imaginary frequencies).[74] Stabilities of the SACs are measured by calculating the interaction energies defined in eq 1:[75]

$$E_{int} = E_{(cage+TM)} - (E_{cage} + E_{TM}) \quad (1)$$

where E_{cage} refers to the energy of the pristine magnesium oxide nanocage, E_{TM} is the energy of the respective transition metal, and $E_{(cage+TM)}$ is the energy of the optimized structure of the designed SACs. By this definition, negative E_{int} values with large magnitudes reflect the stability of the corresponding structure. In other words, the more negative the value is, the more stable the structure is. For electronic analysis, single-point calculations have been performed on the optimized structures at the B3LYP/6-31G + (d,p) level of theory. The B3LYP functional has been chosen based on the literature as it is well accepted that the B3LYP functional provides data that agree with experimental electronic analysis results.[76−78]

The difference in energy between FMOs has been calculated using eq 2:[79]

$$E_{gap} = E_{LUMO} - E_{HOMO} \quad (2)$$

where E_{gap} is the difference in energy between the HOMO and the LUMO, E_{LUMO} is the energy of the LUMO, and E_{HOMO} is the energy of the HOMO. The Multiwfn 3.80 code[80] was utilized in performing the DOS analysis using the wavefunction produced at the B3LYP/6-31G + (d,p) level of theory. The DOS analysis was done on all structures to obtain information about the position of orbitals before and after the decoration with the TMs.

Theoretically, the main activity descriptor for the HER is the Gibbs free energy of hydrogen evolution (ΔG_{H^*}); it is sometimes called the "HER activity descriptor".[14,26,81] Large positive values of ΔG_{H^*} indicate that adsorption of hydrogen is highly unfavorable, whereas large negative values of ΔG_{H^*} correspond to having hydrogen adsorbed strongly. This results in difficulties in desorbing hydrogen to produce H_2, thus hindering the catalytic activity. Therefore, having ΔG_{H^*} as close to zero as possible makes for an excellent catalyst. The overall HER mechanism pathway contains the following half-cell reaction:

$$H^{+}_{(aq)} + e^{-} \rightarrow \frac{1}{2}H_{2(g)} \quad (3)$$

Under standard conditions, the Gibbs free energy of $H^{+}_{(aq)} + e^{-}$ is equal to half that of $H_{2(g)}$. By definition, the Gibbs free energy of this reaction is taken as zero. Therefore, the Gibbs free energy of reactants is equal to that of products. Hence, to

https://doi.org/10.1021/acsomega.3c01794
ACS Omega 2023, 8, 37820−37829

calculate the ΔG_{H^*}, computed data of $H_{2(g)}$ are used. The Gibbs free energies of hydrogen evolution are calculated using eq 4:[55,82−88]

$$\Delta G_{H^*} = \Delta E_{H^*} + \Delta E_{ZPE} - T\Delta S_{H^*} \quad (4)$$

where ΔE_{H^*} is the hydrogen adsorption energy, ΔE_{ZPE} is the difference in zero-point energies of hydrogen adsorption, T is the temperature, which has been set as 298.15 K, and ΔS_{H^*} is the difference in entropy of hydrogen adsorption. ΔE_{H^*} is calculated using eq 5:[40,55,83,84,86−89]

$$\Delta E_{H^*} = E_{(cage+TM+H)} - \left(E_{(cage+TM)} + \frac{1}{2}E_{H2}\right) \quad (5)$$

where $E_{(cage+TM+H)}$ is the energy of the intermediate and E_{H2} is the energy of the hydrogen molecule. ΔE_{ZPE} can be calculated using eq 6:[83,84,86−88]

$$\Delta E_{ZPE} = E_{ZPE(cage+TM+H)} - \left(E_{ZPE(cage+TM)} + \frac{1}{2}E_{ZPE(H2)}\right) \quad (6)$$

where $E_{ZPE(cage+TM+H)}$ is the zero-point energy of the intermediate, $E_{ZPE(cage+TM)}$ is the zero-point energy of the SAC, and $E_{ZPE(H2)}$ is the zero-point energy of the hydrogen molecule. ΔS_{H^*} can be calculated by eq 7:[84,86−89]

$$\Delta S_{H^*} = S_{(cage+TM+H)} - \left(S_{(cage+TM)} + \frac{1}{2}S_{H2}\right) \quad (7)$$

where $S_{(cage+TM+H)}$ is the absolute entropy of the intermediate, $S_{(cage+TM)}$ is the absolute entropy of the SAC, and $S_{ZPE(H2)}$ is the absolute entropy of the hydrogen molecule. All thermodynamic properties are calculated at 298.15 K and 1.00 atm.

■ ASSOCIATED CONTENT

Supporting Information

The Supporting Information is available free of charge at https://pubs.acs.org/doi/10.1021/acsomega.3c01794.

Graphical representation of the HOMOs and LUMOs of the pristine and TM-doped $Mg_{12}O_{12}$ systems, DOS spectra of the pristine and TM-doped $Mg_{12}O_{12}$ systems, optimized geometries of the OER intermediates, spin state analysis results of the OER intermediates, and Gibbs free energy changes of the PCET steps (PDF)

■ AUTHOR INFORMATION

Corresponding Authors

Nadeem S. Sheikh − *Chemical Sciences, Faculty of Science, Universiti Brunei Darussalam, Gadong BE1410, Brunei Darussalam*; orcid.org/0000-0002-0716-7562; Email: nadeem.sheikh@ubd.edu.bn

Tariq Mahmood − *Department of Chemistry, College of Science, University of Bahrain, Sakhir 32038, Bahrain; Department of Chemistry, COMSATS University Islamabad, Abbottabad 22060, Pakistan*; orcid.org/0000-0001-8850-9992; Email: tmahmood@uob.edu.bh

Authors

Abdulrahman Allangawi − *Department of Chemistry, College of Science, University of Bahrain, Sakhir 32038, Bahrain*; orcid.org/0000-0001-7353-9312

Naveen Kosar − *Department of Chemistry, COMSATS University Islamabad, Lahore 54000, Pakistan*

Khurshid Ayub − *Department of Chemistry, COMSATS University Islamabad, Abbottabad 22060, Pakistan*; orcid.org/0000-0003-0990-1860

Mazhar Amjad Gilani − *Department of Chemistry, COMSATS University Islamabad, Lahore 00000, Pakistan*

Nur Hazimah Binti Zainal Arfan − *Chemical Sciences, Faculty of Science, Universiti Brunei Darussalam, Gadong BE1410, Brunei Darussalam*

Malai Haniti Sheikh Abdul Hamid − *Chemical Sciences, Faculty of Science, Universiti Brunei Darussalam, Gadong BE1410, Brunei Darussalam*

Muhammad Imran − *Department of Chemistry, Faculty of Science, King Khalid University, Abha 61413, Saudi Arabia*

Complete contact information is available at: https://pubs.acs.org/10.1021/acsomega.3c01794

Notes

The authors declare no competing financial interest.

■ ACKNOWLEDGMENTS

N.H.B.Z.A., M.H.S.A.H., and N.S.S. thank the Universiti Brunei Darussalam for the FIC research grant (UBD/RSCH/1.4/FICBF(b)/2022/049) and the allied research grant. M.I. expresses appreciation to the Deanship of Scientific Research at King Khalid University Saudi Arabia through the research groups' program under Grant Number R.G.P. 2/256/44. A.A. and T.M. acknowledge the University of Bahrain, Higher Education Commission of Pakistan, and COMSATS University Islamabad, Abbottabad Campus for financial support.

■ REFERENCES

(1) Johari, A.; Singh, S.; Vidya, S. Engine performance analysis for diesel engine using hydrogen as an alternative fuel. *Mater. Today: Proc.* **2022**, *56*, 342−346.

(2) Abeleda, J. M. A., Jr.; Espiritu, R. The status and prospects of hydrogen and fuel cell technology in the Philippines. *Energy Policy* **2022**, *162*, No. 112781.

(3) Lee, Y.; Lee, M. C.; Kim, Y. J. Barriers and strategies of hydrogen fuel cell power generation based on expert survey in South Korea. *Int. J. Hydrogen Energy* **2022**, *47*, 5709−5719.

(4) Ferraren-De Cagalitan, D. D. T.; Abundo, M. L. S. A review of biohydrogen production technology for application towards hydrogen fuel cells. *Renew. Sustain. Energy Rev.* **2021**, *151*, No. 111413.

(5) Sapountzi, F. M.; Gracia, J. M.; Weststrate, C. J.; Fredriksson, H. O. A.; Niemantsverdriet, J. W. Electrocatalysts for the generation of hydrogen, oxygen and synthesis gas. *Prog. Energy Combust. Sci.* **2017**, *58*, 1−35.

(6) Bonaccorso, F.; Colombo, L.; Yu, G.; Stoller, M.; Tozzini, V.; Ferrari, A. C.; Ruoff, R. S.; Pellegrini, V. Graphene, related two-dimensional crystals, and hybrid systems for energy conversion and storage. *Science* **2015**, *347*, No. 1246501.

(7) Acar, C.; Dincer, I.; Naterer, G. F. Review of photocatalytic water-splitting methods for sustainable hydrogen production. *Int. J. Energy Res.* **2016**, *40*, 1449−1473.

(8) Felseghi, R.-A.; Carcadea, E.; Raboaca, M. S.; Trufin, C. N.; Filote, C. Hydrogen Fuel Cell Technology for the Sustainable Future of Stationary Applications. *Energies* **2019**, *12*, 4593.

(9) Alves, H. J.; Junior, C. B.; Niklevicz, R. R.; Frigo, E. P.; Frigo, M. S.; Coimbra-Araújo, C. H. Overview of hydrogen production technologies from biogas and the applications in fuel cells. *Int. J. Hydrogen Energy* **2013**, *38*, 5215−5225.

(10) Mahecha-Botero, A.; Boyd, T.; Gulamhusein, A.; Grace, J. R.; Lim, C. J.; Shirasaki, Y.; Kurokawa, H.; Yasuda, I. Catalytic reforming of natural gas for hydrogen production in a pilot fluidized-bed

membrane reactor: Mapping of operating and feed conditions. *Int. J. Hydrogen Energy* **2011**, *36*, 10727−10736.
(11) Jusino, A.; Schobert, H. H. The use of sulfur to extract hydrogen from coal. *Int. J. Coal Geol.* **2006**, *65*, 223−234.
(12) Deng, Z.-Y.; Ferreira, J. M. F.; Sakka, Y. Hydrogen-Generation Materials for Portable Applications. *J. Am. Ceram. Soc.* **2008**, *91*, 3825−3834.
(13) de Souza, R. F.; Padilha, J. C.; Gonçalves, R. S.; de Souza, M. O.; Rault-Berthelot, J. Electrochemical hydrogen production from water electrolysis using ionic liquid as electrolytes: Towards the best device. *J. Power Sources* **2007**, *164*, 792−798.
(14) Zou, X.; Zhang, Y. Noble metal-free hydrogen evolution catalysts for water splitting. *Chem. Soc. Rev.* **2015**, *44*, 5148−5180.
(15) Zeng, K.; Zhang, D. Recent progress in alkaline water electrolysis for hydrogen production and applications. *Prog. Energy Combust. Sci.* **2010**, *36*, 307−326.
(16) Zhao, D.; Zhuang, Z.; Cao, X.; Zhang, C.; Peng, Q.; Chen, C.; Li, Y. Atomic site electrocatalysts for water splitting, oxygen reduction and selective oxidation. *Chem. Soc. Rev.* **2020**, *49*, 2215−2264.
(17) Li, Y.; Wei, X.; Chen, L.; Shi, J. Electrocatalytic Hydrogen Production Trilogy. *Angew. Chem., Int. Ed.* **2021**, *60*, 19550−19571.
(18) Inamdar, A. I.; Chavan, H. S.; Hou, B.; Lee, C. H.; Lee, S. U.; Cha, S.; Kim, H.; Im, H. A Robust Nonprecious CuFe Composite as a Highly Efficient Bifunctional Catalyst for Overall Electrochemical Water Splitting. *Small* **2020**, *16*, No. 1905884.
(19) Li, D.; Xu, Y.; Lu, Y.; Chen, Y.; Wu, Y.; Yan, J.; Du, F.; Zhao, Y.; Tan, X. Defect-rich engineering of Ni-incorporated tungsten oxides micro-flowers on carbon cloth: A binder-free electrode for highly efficient hydrogen evolution reaction. *J. Power Sources* **2022**, *520*, No. 230862.
(20) Li, F.; Han, G.-F.; Bu, Y.; Chen, S.; Ahmad, I.; Jeong, H. Y.; Fu, Z.; Lu, Y.; Baek, J.-B. Unveiling the critical role of active site interaction in single atom catalyst towards hydrogen evolution catalysis. *Nano Energy* **2022**, *93*, No. 106819.
(21) Zhu, J.; Yang, R.; Zhang, G. Atomically thin transition metal dichalcogenides for the hydrogen evolution reaction. *ChemPhysMater* **2022**, *1*, 102−111.
(22) Feng, C.; Xin, B.; Li, H.; Jia, Z.; Zhang, X.; Geng, B. Agaric-like cobalt diselenide supported by carbon nanofiber as an efficient catalyst for hydrogen evolution reaction. *J. Colloid Interface Sci.* **2022**, *610*, 854−862.
(23) Zhang, S.; Li, P.; Yue, L.; Wu, X.; Wang, J.; Ren, H.; Hao, Z.; Chen, T.; Wang, L.; Wu, M. A kind of electro-catalyst with high efficiency for hydrogen evolution reaction: Platinum particles dispersed on multi-walled carbon nanotubes. *Mater. Lett.* **2022**, *312*, No. 131704.
(24) Wang, B.; Tang, C.; Wang, H.-F.; Chen, X.; Cao, R.; Zhang, Q. A Nanosized CoNi Hydroxide@Hydroxysulfide Core−Shell Heterostructure for Enhanced Oxygen Evolution. *Adv. Mater.* **2019**, *31*, No. e1805658.
(25) Zhu, H.; Ren, X.; Yang, X.; Liang, X.; Liu, A.; Wu, G. Fe-based catalysts for nitrogen reduction toward ammonia electrosynthesis under ambient conditions. *SusMat* **2022**, *2*, 214−242.
(26) Aggarwal, P.; Sarkar, D.; Awasthi, K.; Menezes, P. W. Functional role of single-atom catalysts in electrocatalytic hydrogen evolution: Current developments and future challenges. *Coord. Chem. Rev.* **2022**, *452*, No. 214289.
(27) Wang, A.; Li, J.; Zhang, T. Heterogeneous single-atom catalysis. *Nat. Rev. Chem.* **2018**, *2*, 65−81.
(28) Li, J.; Stephanopoulos, M. F.; Xia, Y. Introduction: Heterogeneous Single-Atom Catalysis. *Chem. Rev.* **2020**, *120*, 11699−11702.
(29) Khan, M. A.; Zhao, H.; Zou, W.; Chen, Z.; Cao, W.; Fang, J.; Xu, J.; Zhang, L.; Zhang, J. Recent Progresses in Electrocatalysts for Water Electrolysis. *Electrochem. Energy Rev.* **2018**, *1*, 483−530.
(30) Tiwari, J. N.; Sultan, S.; Myung, C. W.; Yoon, T.; Li, N.; Ha, M.; Harzandi, A. M.; Park, H. J.; Kim, D. Y.; Chandrasekaran, S. S.; et al. Multicomponent electrocatalyst with ultralow Pt loading and high hydrogen evolution activity. *Nat. Energy* **2018**, *3*, 773−782.
(31) Cheng, X.; Lu, Y.; Zheng, L.; Cui, Y.; Niibe, M.; Tokushima, T.; Li, H.; Zhang, Y.; Chen, G.; Sun, S.; et al. Charge redistribution within platinum−nitrogen coordination structure to boost hydrogen evolution. *Nano Energy* **2020**, *73*, No. 104739.
(32) Lim, T.; Kim, S.-K. Non-precious hydrogen evolution reaction catalysts: Stepping forward to practical polymer electrolyte membrane-based zero-gap water electrolyzers. *Chem. Eng. J.* **2022**, *433*, No. 133681.
(33) Hughes, J. P.; Clipsham, J.; Chavushoglu, H.; Rowley-Neale, S. J.; Banks, C. E. Polymer electrolyte electrolysis: A review of the activity and stability of non-precious metal hydrogen evolution reaction and oxygen evolution reaction catalysts. *Renew. Sustain. Energy Rev.* **2021**, *139*, No. 110709.
(34) Sun, Y.; Zhang, T.; Li, C.; Xu, K.; Li, Y. Compositional engineering of sulfides, phosphides, carbides, nitrides, oxides, and hydroxides for water splitting. *J. Mater. Chem. A* **2020**, *8*, 13415−13436.
(35) Yang, Y.; Liang, Y.; Guo, M.; Yu, T.; Xu, K.; Lu, L.; Yuan, C. Controllable synthesis of one-dimensional NiS2 nanotube and nanorod arrays on nickel foams for efficient electrocatalytic water splitting. *Int. J. Hydrogen Energy* **2021**, *46*, 50−60.
(36) Qiu, H.-J.; Ito, Y.; Cong, W.; Tan, Y.; Liu, P.; Hirata, A.; Fujita, T.; Tang, Z.; Chen, M. Nanoporous Graphene with Single-Atom Nickel Dopants: An Efficient and Stable Catalyst for Electrochemical Hydrogen Production. *Angew. Chem., Int. Ed.* **2015**, *54*, 14031−14035.
(37) Harzandi, A. M.; Shadman, S.; Ha, M.; Myung, C. W.; Kim, D. Y.; Park, H. J.; Sultan, S.; Noh, W.-S.; Lee, W.; Thangavel, P.; Byun, W. J.; Lee, S. H.; Tiwari, J. N.; Shin, T. J.; Park, J. H.; Lee, Z.; Lee, J. S.; Kim, K. S. Immiscible bi-metal single-atoms driven synthesis of electrocatalysts having superb mass-activity and durability. *Appl. Catal., B* **2020**, *270*, No. 118896.
(38) Fei, H.; Dong, J.; Arellano-Jiménez, M. J.; Ye, G.; Dong Kim, N.; Samuel, E. L. G.; Peng, Z.; Zhu, Z.; Qin, F.; Bao, J.; et al. Atomic cobalt on nitrogen-doped graphene for hydrogen generation. *Nat. Commun.* **2015**, *6*, 8668.
(39) Shen, Z.; Fan, X.; Ma, S.; An, Y.; Yang, D.; Guo, N.; Luo, Z.; Hu, Y. 3d transitional-metal single atom catalysis toward hydrogen evolution reaction on MXenes supports. *Int. J. Hydrogen Energy* **2020**, *45*, 14396−14406.
(40) Sun, Z.; Gao, Z.; Xu, X.; Tao, J.; Guan, L. Low-cost single-atom transition metals on two-dimensional SnO nanosheets for efficient hydrogen evolution catalysis in all pH-range. *Appl. Surf. Sci.* **2022**, *578*, No. 152021.
(41) Lu, B.; Liu, Q.; Chen, S. Electrocatalysis of Single-Atom Sites: Impacts of Atomic Coordination. *ACS Catal.* **2020**, *10*, 7584−7618.
(42) Piccolo, L. Restructuring effects of the chemical environment in metal nanocatalysis and single-atom catalysis. *Catal. Today* **2021**, *373*, 80−97.
(43) Liu, G.; Robertson, A. W.; Li, M. M.-J.; Kuo, W. C. H.; Darby, M. T.; Muhieddine, M. H.; Lin, Y.-C.; Suenaga, K.; Stamatakis, M.; Warner, J. H.; et al. MoS2 monolayer catalyst doped with isolated Co atoms for the hydrodeoxygenation reaction. *Nat. Chem.* **2017**, *9*, 810−816.
(44) Liu, J.-C.; Wang, Y.-G.; Li, J. Toward Rational Design of Oxide-Supported Single-Atom Catalysts: Atomic Dispersion of Gold on Ceria. *J. Am. Chem. Soc.* **2017**, *139*, 6190−6199.
(45) Zhao, Z.; Li, Z.; Wang, Q.; Shi, T.-T. Structures, electronic and magnetic properties of transition metal atoms encapsulated in Mg12O12 nanocage. *Mater. Chem. Phys.* **2020**, *240*, No. 122220.
(46) Javan, M. B. Magnetic properties of Mg12O12 nanocage doped with transition metal atoms (Mn, Fe, Co and Ni): DFT study. *J. Magn. Magn. Mater.* **2015**, *385*, 138−144.
(47) Fallahi, P.; Jouypazadeh, H.; Farrokhpour, H. Theoretical studies on the potentials of some nanocages (Al12N12, Al12P12, B12N12, Be12O12, C12Si12, Mg12O12 and C24) on the detection and adsorption of Tabun molecule: DFT and TD-DFT study. *J. Mol. Liq.* **2018**, *260*, 138−148.

https://doi.org/10.1021/acsomega.3c01794
ACS Omega 2023, 8, 37820−37829

(48) Kakemam, J.; Peyghan, A. A. Electronic, energetic, and structural properties of C-and Si-doped Mg12O12 nano-cages. *Comput. Mater. Sci.* **2013**, *79*, 352−355.
(49) Shakerzdeh, E.; Tahmasebi, E.; Shamlouei, H. R. The influence of alkali metals (Li, Na and K) interaction with Be12O12 and Mg12O12 nanoclusters on their structural, electronic and nonlinear optical properties: A theoretical study. *Synth. Met.* **2015**, *204*, 17−24.
(50) Ghorbanzadeh Ahangari, M.; Hamed Mashhadzadeh, A. Density functional theory based molecular dynamics study on hydrogen storage capacity of C24, B12N12, Al12 N12, Be12O12, Mg12O12, and Zn12O12 nanocages. *Int. J. Hydrogen Energy* **2020**, *45*, 6745−6756.
(51) Hussain, S.; Chatha, S. A. S.; Hussain, A. I.; Hussain, R.; Yasir Mehboob, M.; Mansha, A.; Shahzad, N.; Ayub, K. A Theoretical Framework of Zinc-Decorated Inorganic Mg12O12 Nanoclusters for Efficient COCl2 Adsorption: A Step Forward toward the Development of COCl2 Sensing Materials. *ACS Omega* **2021**, *6*, 19435−19444.
(52) Weller, M. T.; Overton, T.; Armstrong, F.; Rourke, J. *Inorganic Chemistry*; Oxford University Press, 2018.
(53) Hu, J.; Li, Y.; Zou, Y.; Lin, L.; Li, B.; Li, X.-Y. Transition metal single-atom embedded on N-doped carbon as a catalyst for peroxymonosulfate activation: A DFT study. *Chem. Eng. J.* **2022**, *437*, No. 135428.
(54) Butt, M. H.; Zaidi, S. H. M.; Nabeela; Khan, A.; Ayub, K.; Yar, M.; Hashmi, M. A.; Yawer, M. A.; Zia, M. A. Cu-doped phosphorene as highly efficient single atom catalyst for CO oxidation: A DFT study. *Mol. Catal.* **2021**, *509*, No. 111630.
(55) Gao, F.; Wei, Y.; Du, J.; Jiang, G. Theoretical screening of 2D materials supported transition-metal single atoms as efficient electrocatalysts for hydrogen evolution reaction. *Materialia* **2021**, *18*, No. 101168.
(56) Ye, Z.; Xie, S.; Cao, Z.; Wang, L.; Xu, D.; Zhang, H.; Matz, J.; Dong, P.; Fang, H.; Shen, J.; et al. High-rate aqueous zinc-organic battery achieved by lowering HOMO/LUMO of organic cathode. *Energy Storage Mater.* **2021**, *37*, 378−386.
(57) El-Gharkawy, E.-S. R.; Ammar, H. Adsorption of CO on TM-deposited (MgO) 12 nano-Cage (TM= Ni, Pd and Pt): a study on electronic properties. *J. Nanoelectron. Optoelectron.* **2018**, *13*, 546−553.
(58) Jouypazadeh, H.; Farrokhpour, H. DFT and TD-DFT study of the adsorption and detection of sulfur mustard chemical warfare agent by the C24, C12Si12, Al12N12, Al12P12, Be12O12, B12N12 and Mg12O12 nanocages. *J. Mol. Struct.* **2018**, *1164*, 227−238.
(59) Shamlouei, H. R.; Nouri, A.; Mohammadi, A.; Tehrani, A. D. Influence of transition metal atoms doping on structural, electronic and nonlinear optical properties of Mg12O12 nanoclusters: A DFT study. *Phys. E: Low-Dimens. Syst. Nanostruct.* **2016**, *77*, 48−53.
(60) Glendening, E.; Reed, A.; Carpenter, J.; Weinhold, F. *NBO, version 3.1*; Gaussian. Inc.: Pittsburgh, PA, 2003.
(61) Carpenter, J. E. *Extension of Lewis structure concepts to open-shell and excited-state molecular species*; University of Wisconsin--Madison, 1987.
(62) Irshad, S.; Ullah, F.; Khan, S.; Ludwig, R.; Mahmood, T.; Ayub, K. First row transition metals decorated boron phosphide nanoclusters as nonlinear optical materials with high thermodynamic stability and enhanced electronic properties; A detailed quantum chemical study. *Opt. Laser Technol.* **2021**, *134*, No. 106570.
(63) Prins, R. Hydrogen spillover. Facts and fiction. *Chem. Rev.* **2012**, *112*, 2714−2738.
(64) Ullah, F.; Ayub, K.; Mahmood, T. High performance SACs for HER process using late first-row transition metals anchored on graphyne support: A DFT insight. *Int. J. Hydrogen Energy* **2021**, *46*, 37814−37823.
(65) Pan, Y.; Liu, S.; Sun, K.; Chen, X.; Wang, B.; Wu, K.; Cao, X.; Cheong, W.-C.; Shen, R.; Han, A.; Chen, Z.; Zheng, L.; Luo, J.; Lin, Y.; Liu, Y.; Wang, D.; Peng, Q.; Zhang, Q.; Chen, C.; Li, Y. A Bimetallic Zn/Fe Polyphthalocyanine-Derived Single-Atom Fe-N4 Catalytic Site: A Superior Trifunctional Catalyst for Overall Water Splitting and Zn−Air Batteries. *Angew. Chem., Int. Ed.* **2018**, *57*, 8614−8618.
(66) Xue, Y.; Huang, B.; Yi, Y.; Guo, Y.; Zuo, Z.; Li, Y.; Jia, Z.; Liu, H.; Li, Y. Anchoring zero valence single atoms of nickel and iron on graphdiyne for hydrogen evolution. *Nat. Commun.* **2018**, *9*, 1460.
(67) Wang, L.; Liu, X.; Cao, L.; Zhang, W.; Chen, T.; Lin, Y.; Wang, H.; Wang, Y.; Yao, T. Active Sites of Single-Atom Iron Catalyst for Electrochemical Hydrogen Evolution. *J. Phys. Chem. Lett.* **2020**, *11*, 6691−6696.
(68) Allangawi, A.; Mahmood, T.; Ayub, K.; Gilani, M. A. Anchoring the late first row transition metals with B12P12 nanocage to act as single atom catalysts toward oxygen evolution reaction (OER). *Mater. Sci. Semicond. Process.* **2023**, *153*, No. 107164.
(69) An, L.; Wei, C.; Lu, M.; Liu, H.; Chen, Y.; Scherer, G. G.; Fisher, A. C.; Xi, P.; Xu, Z. J.; Yan, C. H. Recent development of oxygen evolution electrocatalysts in acidic environment. *Adv. Mater.* **2021**, *33*, No. 2006328.
(70) Rossmeisl, J.; Qu, Z. W.; Zhu, H.; Kroes, G. J.; Nørskov, J. K. Electrolysis of water on oxide surfaces. *J. Electroanal. Chem.* **2007**, *607*, 83−89.
(71) Frisch, M.; Trucks, G.; Schlegel, H.; Scuseria, G.; Robb, M.; Cheeseman, J.; Scalmani, G.; Barone, V.; Mennucci, B.; Petersson, G. *Gaussian 09, rev. D. 01*; Gaussian Inc.: Wallingford CT 2009.
(72) Dennington, R.; Keith, T.; Millam, J. *GaussView, version 6.0.16*. 2016.
(73) Chai, J.-D.; Head-Gordon, M. Long-range corrected hybrid density functionals with damped atom−atom dispersion corrections. *Phys. Chem. Chem. Phys.* **2008**, *10*, 6615−6620.
(74) Levine, I. N. *Quantum Chemistry*; Pearson, 2014.
(75) Sredojević, D. N.; Belić, M. R.; Šljivančanin, Ž. Hydrogen Evolution Reaction over Single-Atom Catalysts Based on Metal Adatoms at Defected Graphene and h-BN. *J. Phys. Chem. C* **2020**, *124*, 16860−16867.
(76) Sajid, H.; Mahmood, T.; Ayub, K. High sensitivity of polypyrrole sensor for uric acid over urea, acetamide and sulfonamide: A density functional theory study. *Synth. Met.* **2018**, *235*, 49−60.
(77) Ullah, H.; Shah, A.-U.-H. A.; Ayub, K.; Bilal, S. Density Functional Theory Study of Poly(o-phenylenediamine) Oligomers. *J. Phys. Chem. C* **2013**, *117*, 4069−4078.
(78) Ullah, H.; Shah, A.-U.-H. A.; Bilal, S.; Ayub, K. Doping and Dedoping Processes of Polypyrrole: DFT Study with Hybrid Functionals. *J. Phys. Chem. C* **2014**, *118*, 17819−17830.
(79) Khan, P.; Jamshaid, M.; Tabassum, S.; Perveen, S.; Mahmood, T.; Ayub, K.; Yang, J.; Gilani, M. A. Exploring the Interaction of Ionic Liquids with Al12N12 and Al12P12 Nanocages for Better Electrode-Electrolyte Materials in Super Capacitors. *J. Mol. Liq.* **2021**, *344*, No. 117828.
(80) Lu, T.; Chen, F. Multiwfn: A multifunctional wavefunction analyzer. *J. Comput. Chem.* **2012**, *33*, 580−592.
(81) Nørskov, J. K.; Bligaard, T.; Rossmeisl, J.; Christensen, C. H. Towards the computational design of solid catalysts. *Nat. Chem.* **2009**, *1*, 37−46.
(82) Li, W.-Z.; Liu, M.-Y.; Gong, L.; Zhang, M.-L.; Cao, C.; He, Y. The electronic properties and catalytic activity of precious-metals adsorbed silicene for hydrogen evolution reaction and oxygen evolution reaction. *Appl. Surf. Sci.* **2021**, *560*, No. 150041.
(83) Lv, X.; Wei, W.; Zhao, P.; Er, D.; Huang, B.; Dai, Y.; Jacob, T. Oxygen-terminated BiXenes and derived single atom catalysts for the hydrogen evolution reaction. *J. Catal.* **2019**, *378*, 97−103.
(84) Yang, K.; Zhou, G. Hydrogen evolution/spillover effect of single cobalt atom on anatase TiO2 from first-principles calculations. *Appl. Surf. Sci.* **2021**, *536*, No. 147831.
(85) Zhou, W.; Jiang, Z.; Chen, M.; Li, Z.; Luo, X.; Guo, M.; Yang, Y.; Yu, T.; Yuan, C.; Wang, S. Directly anchoring non-noble metal single atoms on 1T-TMDs with tip structure for efficient hydrogen evolution. *Chem. Eng. J.* **2022**, *428*, No. 131210.
(86) Nørskov, J. K.; Rossmeisl, J.; Logadottir, A.; Lindqvist, L.; Kitchin, J. R.; Bligaard, T.; Jónsson, H. Origin of the Overpotential for

https://doi.org/10.1021/acsomega.3c01794
ACS Omega 2023, 8, 37820−37829

Oxygen Reduction at a Fuel-Cell Cathode. *J. Phys. Chem. B* **2004**, *108*, 17886−17892.
(87) Valdés, Á.; Qu, Z. W.; Kroes, G. J.; Rossmeisl, J.; Nørskov, J. K. Oxidation and Photo-Oxidation of Water on TiO2 Surface. *J. Phys. Chem. C* **2008**, *112*, 9872−9879.
(88) Tang, Q.; Jiang, D.-E. Mechanism of Hydrogen Evolution Reaction on 1T-MoS2 from First Principles. *ACS Catal.* **2016**, *6*, 4953−4961.
(89) Bi, H.; Zhang, L.; Wang, Z.; Zhou, G. Identification of active sites available for hydrogen evolution of Single-Atom Ni1/TiO2 catalysts. *Appl. Surf. Sci.* **2022**, *579*, No. 152139.

https://doi.org/10.1021/acsomega.3c01794
ACS Omega 2023, 8, 37820−37829